Advances in
Bridge Engineering

ORIGINAL INNOVATION

Open Access

Aerodynamic interference between two boxes in parallel arrangement and flow field characteristics around the girder

Shuwen Fan[1], Wei Chen[1], Haojun Tang[1,2*] and Yongle Li[1,2]

*Correspondence:
thj@swjtu.edu.cn

[1] Department of Bridge Engineering, Southwest Jiaotong University, Chengdu 610031, China
[2] Wind Engineering Key Laboratory of Sichuan Province, Chengdu 610031, China

Abstract

Aerodynamic characteristics of long-span bridges with box girders have been investigated widely, and this paper presents a study on a cable-stayed bridge with two box girders in parallel arrangement. Computational fluid dynamics (CFD) numerical simulations were adopted to analyze the aerodynamic interference between the upper and the lower box girders. After checking the reliability of the numerical model, different angles of attack and different distances between the two girders were considered, and the variations of the aerodynamic characteristics were discussed, including the aerodynamic coefficients and the static pressure distributions. Then, the wind environment around the two box girders was focused, and the effect on the aerodynamic coefficients of a vehicle was also studied. The results show that the aerodynamic interference between the two box girders is strong, so the aerodynamic characteristics of the two boxes are different from those of a single box. The flow field between the boxes have higher wind velocities, which makes the aerodynamic force on the upper box and the lower box become upward and downward, respectively. Meanwhile, the aerodynamic forces on vehicles above the lower deck surface are larger due to the accelerated flow between the two boxes.

Keywords: Double-deck box girder, Aerodynamic interference, Aerodynamic coefficients, Wind environment, Numerical simulations

1 Introduction

Box girders and truss girders are common types of long-span suspension and cable-stayed bridges. For truss girders, the bridge deck is generally designed above the upper truss members. In some cases, another bridge deck is designed above the lower truss members to increase the traffic capacity. For box girders, a single box with streamlined aerodynamic shapes exhibits good aerodynamic performance and has been widely used. Similar with the truss girder containing two bridge decks, it is supposed that two box girders in parallel arrangement could be designed to increase the traffic capacity.

Aerodynamic forces are important parameters in the design of long-span bridges, and they are related to the girder shape and the inflow direction. Ricciardelli (2003) investigated the wind loading mechanism for a single-box girder. Haque et al (2016)

investigated the shaping effect of a triangular edge fairing on aerodynamic behavior of a bridge deck. Li et al (2018) analyzed aerodynamic coefficients of the streamlined trapezoidal box girder with different wind fairing angles. Liu et al (2022) described a numerical study of the aerodynamic loads produced when a train passed under a bridge and the bridge dynamic response. In order to improve the flutter performance of the bridge, dividing the single box into two separated boxes has been frequently adopted. However, the gap between two parallel boxes complicates the flow field and so do the aerodynamic characteristics of the girder, which has been investigated by many scholars (e.g., Sato et al 2000; Ogawa et al 2002; de Miranda et al 2015; Wu et al 2021). In addition, for two parallel bridges with single-box girders, their aerodynamic characteristics are also related to the aerodynamic interference (Zhou et al 2017; Chen et al 2019; He et al 2021).

The flow field around the girder attracts great attention of scholars, as it determines the aerodynamic forces on the girder and related to the safety of vehicles. Strong crosswinds have a great influence on vehicles travelling through the bridge and may even cause vehicles overturn, sideslip, or other safety problems. For examples in China, seven empty trucks on the Humen Bridge were overturned by strong winds in August 2004. A super long slab truck filled with plastic foam boxes on the Sutong Bridge was overturned in April 2012. A container car on the Qingzhou Bridge was overturned in September 2016. It is of great significance to study the wind environment above the bridge deck. Wang et al (2020), Zhou and Zhu (2020) investigated the wind environment above the bridge deck near the pylon zone and found that the existence of the bridge tower can increase rapidly the wind speed on vehicles. Zhang et al (2020) investigated the local wind environment above the deck of a twin-box girder.

The aforementioned studies mainly focused on a single box or several boxes in tandem arrangements. Due to the limitation of space and the increasing demand for traffic volume, the application of the double-deck truss girder is becoming more and more common, while the double-deck box girder is a relatively new form. Two boxes are arranged in the vertical direction, so the aerodynamic interference between them should be significant. The aerodynamic forces of the girder and the surrounding flow field are different from the situation of a single box girder, calling for further investigation. In this paper, the aerodynamic characteristics of a double-deck box girder are studied using CFD simulations after checking the reliability of the analysis method. The aerodynamic coefficients of the girder with different attack angles of the approaching flow and height distances between the two boxes are computed. The surface pressure distributions around two boxes are also focused to better understand how the aerodynamic interference affects the aerodynamic coefficients. Then, the wind environment above the two boxes and the aerodynamic forces acting on a vehicle are investigated.

2 Aerodynamic coefficients of the double-deck box girder

2.1 CFD model

For the target cable-stayed bridge with a span of 2×210 m, the girder contains two streamlined boxes in parallel arrangement. The upper box is supported by stay cables, which is similar with the single box girder. The lower box is suspended by hangers from the upper one, as shown in Fig. 1.

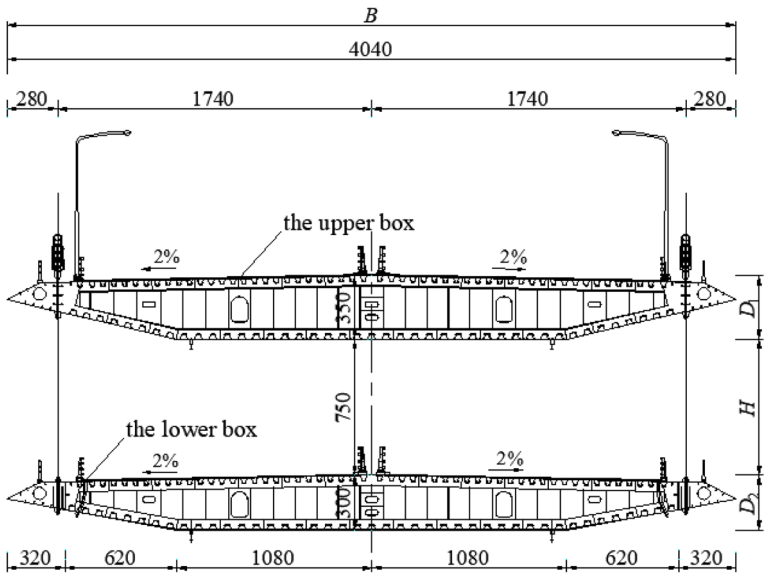

Fig. 1 Cross section of the double-deck box girder (unit: cm)

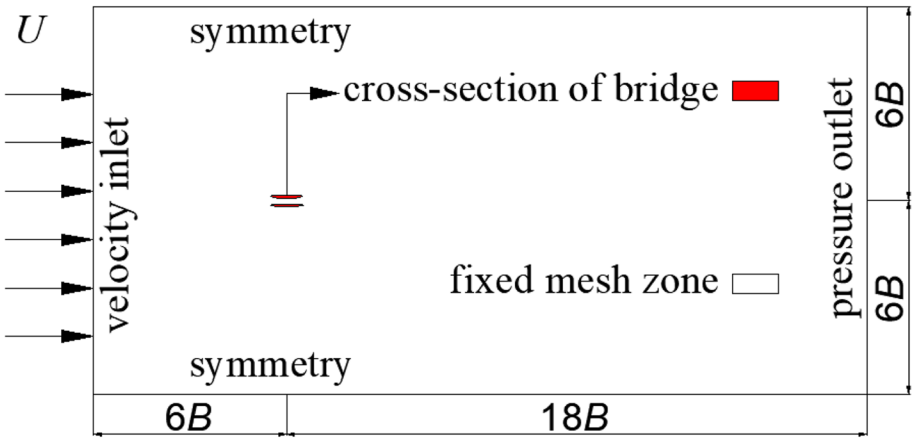

Fig. 2 Computational domain

Two-dimensional (2D) CFD simulations were carried out to investigate the aerodynamic performance of the girder. The computational domain and boundary conditions are shown in Fig. 2. The computational domain is assumed to be 24*B* in the mean-flow direction and 12*B* in the cross-flow direction, where *B* is the width of the upper box. The windward and leeward sides are set as velocity-inlet and pressure-outlet boundaries, respectively. The girders are set as smooth walls. The distance of the bridge center to the velocity inlet boundary is 6*B*. The wind velocity at the inlet is uniform with a turbulence intensity of 0.5% and a turbulent viscosity ratio of 2.0 according to Huang et al. (2009). Local computational mesh employed in numerical analysis is shown in Fig. 3. The computational domain was discretized by quadrilateral meshes, and the cell size progressively increased from the girder to the sides of the domain. In order to improve the efficiency, a near-wall boundary layer with small heights was set clinging to the girder. When the computation was stable, the average of wall *y*-plus values was less than 0.5.

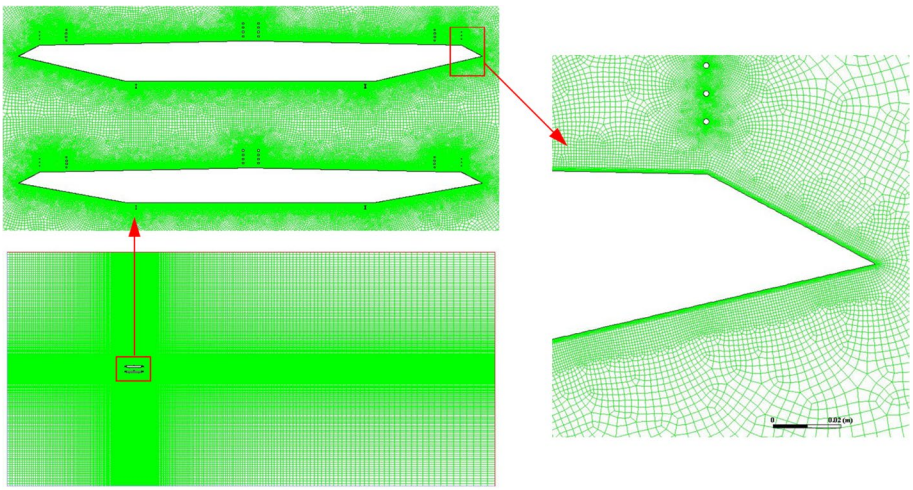

Fig. 3 Local computational mesh employed in numerical simulations

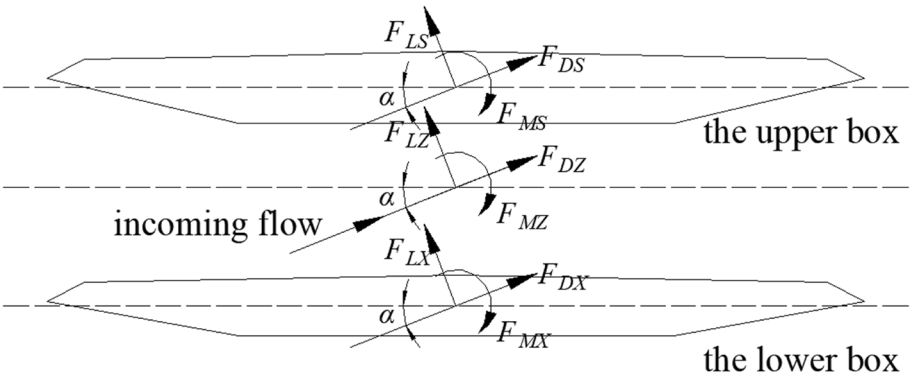

Fig. 4 Definitions of the aerodynamic forces

Unsteady Reynolds-averaged Navier-Stokes (URANS) simulations with a time-step of 10^{-3}s for the 2D model are performed by using the k-ω shear stress transport (SST) model. Such model is known to provide more accurate results, if compared to standard k–ω and k–ε models, in external aerodynamic cases which involve boundary layer separation (de Miranda et al 2015). The SIMPLEC algorithm is employed for pressure-velocity coupling. A second order scheme is selected for pressure, and a second order upwind scheme is selected for momentum, turbulent kinetic energy, and specific dissipation rate. The CFD software FLUENT is used in the simulation.

2.2 Results and discussions

When the angle of attack of the approaching flow is α, the aerodynamic coefficients of the whole cross-section of the girder are defined by Eqs. 1, 2 and 3. The positive directions of the aerodynamic forces are shown in Fig. 4. Besides the whole girder, the aerodynamic forces acting on the upper box and the lower box are also defined, respectively, as shown in Fig. 4.

$$C_D = F_D/\left(0.5\rho U^2 D\right) \tag{1}$$

$$C_L = F_L/\left(0.5\rho U^2 B\right) \tag{2}$$

$$C_M = F_M/\left(0.5\rho U^2 B^2\right) \tag{3}$$

where F_D, F_L and F_M are the drag force, lift force, and moment, respectively; ρ is the air density; B is the girder width; D is the height of the section; U is the mean wind velocity and set as 15 m/s here. As shown in Fig. 1, D corresponds to D_1 or D_2 when calculating the results of the upper or the lower box and (D_1+D_2) when calculating the results of the whole girder.

First, only the upper box was considered and the aerodynamic coefficients were calculated covering the angles of attack from $-10°$ to 10°, as shown in Fig. 5. The results are compared with those of the second Humen Bridge (Fang 2014), as the two cross sections are similar with each other. It can be seen from Fig. 5 that the aerodynamic coefficients of the upper box with the CFD simulations are consistent with the results of the second Humen Bridge with wind tunnel tests. The drag coefficients of the two cases increase rapidly when the absolute value of the angle of attack is large. The lift and the moment coefficients show increasing trends with the increasing angle of attack. Negative slopes could be observed at larger absolute angles of attack.

Subsequently, both the upper and the lower boxes were considered, and the same range of the angle of attack was considered. Figure 6 shows the variations of the aerodynamic coefficients for different cases. For the single upper box and the single lower box, their aerodynamic coefficients versus the angle of attack show similar variations with each other, as shown by the black lines. When the two boxes are arranged together, the results of the upper box and the lower box change significantly due to the aerodynamic interference, as shown by red lines. The drag coefficient of the lower box is larger when the angle of attack is larger or equal to 2°, but it becomes smaller when the angle of attack exceeds 7°. The opposite trend is observed at negative angles of attack. The lift coefficient of the upper box is always larger than that of the lower box, and the variation

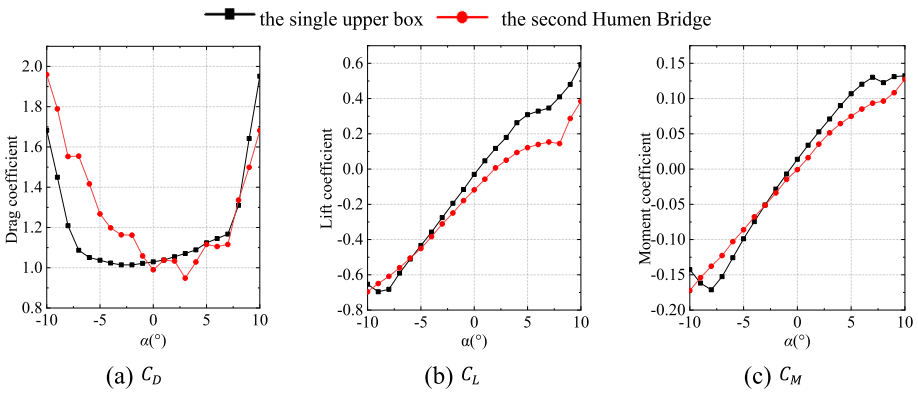

(a) C_D (b) C_L (c) C_M

Fig. 5 Aerodynamic coefficients of the upper box and another box girder

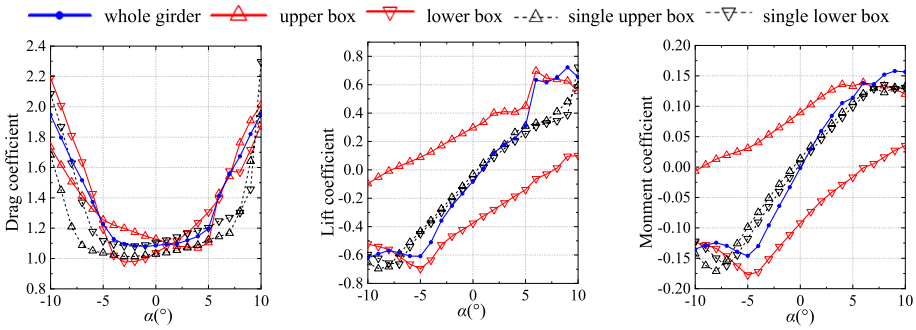

(a) C_D (b) C_L (c) C_M

Fig. 6 Aerodynamic coefficients of the double-deck box girder

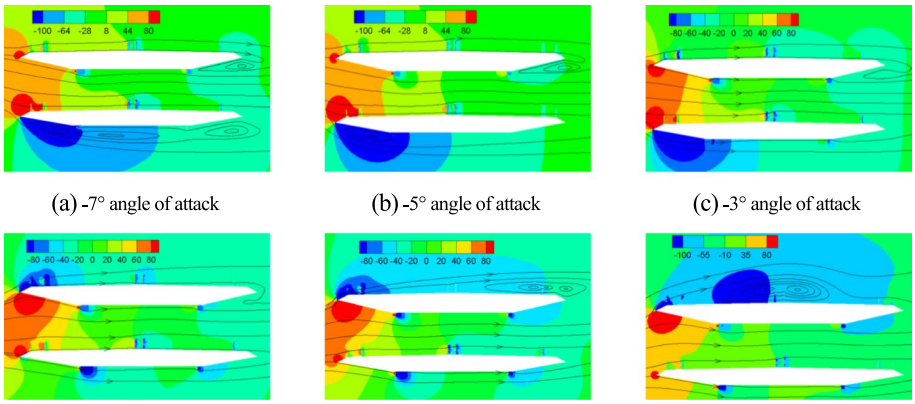

(a) -7° angle of attack (b) -5° angle of attack (c) -3° angle of attack

(d) +3° angle of attack (e) +5° angle of attack (f) +7° angle of attack

Fig. 7 Contours of the static pressure around the two boxes at different angles of attack

of the moment coefficient is similar to the lift coefficient. For the whole girder, however, the variations of the aerodynamic coefficients are similar with those of the single box, as shown by the blue lines.

Figure 7 shows the contours of the static pressure around the two boxes at different angles of attack. At a smaller angle of attack, the box girder exhibits the aerodynamic characteristics of a streamlined body. At a larger angle of attack, the aerodynamic characteristics of a bluff body could observed that the inflow separates from the wind fairing to generate a large vortex above the upper box for positive angles or below the lower box for negative angles.

3 Aerodynamic interference between the two boxes

In order to better understand the aerodynamic interference performance, the distance between the two boxes was changed. Taking the null angle of attack as an example, the distance between the upper and the lower boxes H was decreased from 7.5 m to 7 m and 6 m, and increased to 8 m, 9 m, 10 m, 11 m, 14 m, 17.5 m, and 21 m, respectively. The corresponding distance ratio H/D_1 ranged from 1.71 to 6. For these cases, 2D CFD models were established, and the aerodynamic coefficients were computed. The results are

shown in Fig. 8 where the x-coordinate of 0 represents the case with the single box girder.

The lift coefficients of the single upper and the single lower boxes are close to zero. In the parallel arrangement, however, the aerodynamic interference between the two boxes has strong effects on the lift coefficients, which is related to the distance ratio. With $H/D_1 = 1.71$, the lift force of the upper box becomes upward and the coefficient increases from -0.03 to 0.34, while that of the lower box becomes downward and the coefficient decreases from -0.07 to -0.43. With the increase in H/D_1, a larger distance weakens the aerodynamic interference, so the absolute values of the lift coefficients gradually decrease. Even when H/D_1 increases to 6, the absolute values are still larger than zero. As the lift forces of the upper and the lower boxes are opposite, the coefficient of the whole girder is less affected by H/D_1 and close to zero. The drag and the moment coefficients have the similar variations.

In order to better discuss the aerodynamic interference, the contours of the static pressure around the two boxes with different distances are shown in Fig. 9. The flow field around the double-deck box girder shows different characteristics from that around the single upper or lower box. A big positive pressure region is formed between the two boxes. The static pressure is larger at the windward side, while it decreases along the flow direction towards the leeward side. With the increase in distance between the two boxes, the size of the positive pressure region is enlarged while the values become small. Larger values are observed around the wind fairings at the windward side of the two boxes. Negative pressure regions are formed above the upper box and below the lower box. Above the upper box surface, negative pressure with larger absolute values is formed when the flow is blocked by the crash barriers at the windward and the middle locations. Below the lower box surface, negative pressure with larger absolute values is formed around the corners. With the increase in distance between the two boxes, the aerodynamic interference between the two boxes becomes weak. The sizes of the negative pressure regions are reduced. Larger absolute values are observed around partial crash barriers above the two boxes and the windward corners below the two boxes, which is similar with the flow field around the single upper or lower box.

With different distances, the static pressure distributions around the upper box are shown in Fig. 10. The positive and negative values perform as extrusion and suction,

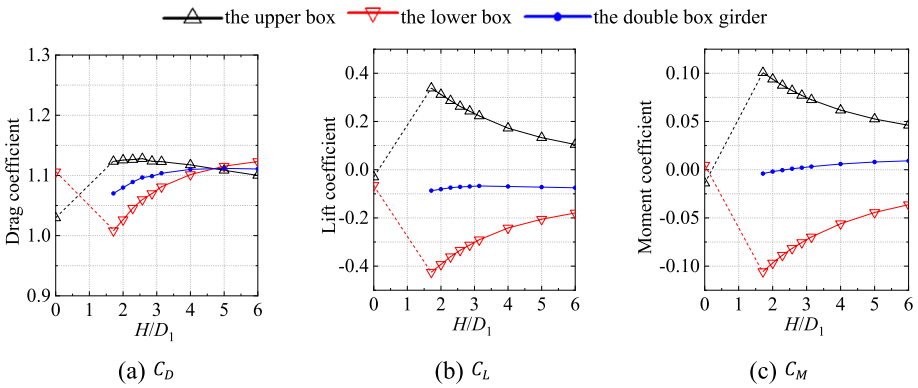

Fig. 8 Aerodynamic coefficients the double box girder with different distance ratios

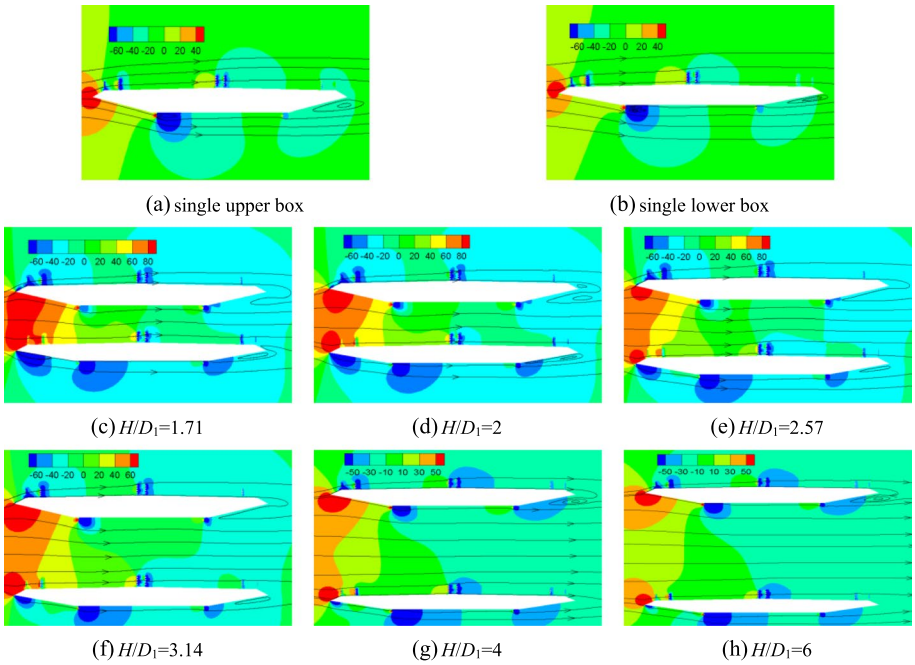

Fig. 9 Contours of the static pressure around the two boxes with different distances (unit: Pa)

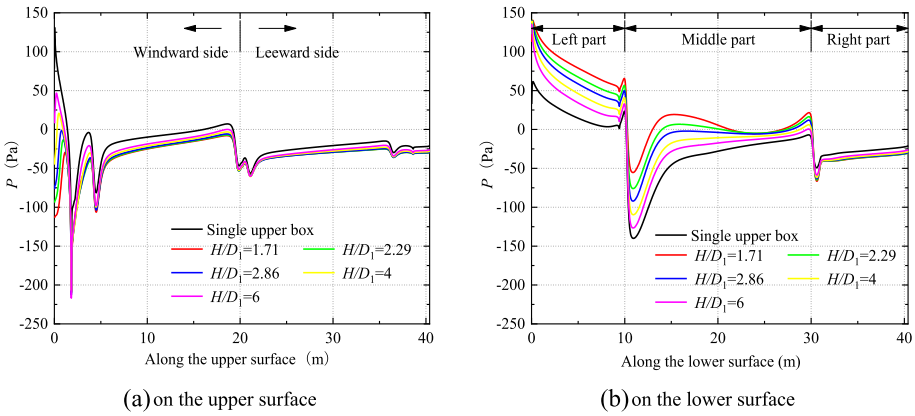

Fig. 10 Distributions of the static pressure on the upper box

respectively. The pressure distributions on the lower surface are easier to affect by the aerodynamic interference than those on the upper surface. Dividing the lower surface into three parts according to the corners, the positive pressure on the left part largely increases when $H/D_1 = 1.71$ and gradually decreases with the increase in H/D_1. The negative pressure on the middle part has smaller absolute values and even becomes positive at some places when $H/D_1 = 1.71$, which recovers gradually with the increase in H/D_1. The negative pressure on the right part is less affected by the change in H/D_1. As a result, the lift coefficient of the upper box becomes upward when the two boxes are arranged together, and it decreases with the increasing distance between the two boxes.

With different distances, the static pressure distributions around the lower box are shown in Fig. 11. The pressure distributions on both the upper and lower surfaces are significantly affected by the aerodynamic interference. On the upper surface, the negative pressure on the windward side becomes positive when $H/D_1 = 1.71$ and recovers gradually with the increase in H/D_1. The pressure distributions on the leeward side are less affected. On the lower surface, the positive pressure on the left part becomes negative even when $H/D_1 = 6$, indicating that the aerodynamic interference still cannot be ignored. The negative pressure on the middle and right part decreases slightly. As a result, the lift coefficient of the lower box becomes downward when the two boxes are arranged together, and it increases with the increasing distance between the two boxes.

4 Flow field characteristics around the girder

4.1 Wind environment above the decks

Flow field characteristics around the girder are not only related to the aerodynamic performance of the bridge itself, but also related to the safety of the vehicles travelling over the bridge. Taking the null angle of attack as the example, the wind environment above the six lanes of the upper box and the six lanes of the lower box, as shown in Fig. 12, is focused.

The wind profiles along the central lines of all lanes are shown in Fig. 13 where V is the mean streamwise velocity at the prototype height y above the deck surface and normalized by the inflow velocity U. The height y is also normalized by the height of the upper box D_1 and the lower box D_2, respectively. With the increase in distance between the two boxes, the wind profiles for the six lanes above the upper box keep similar, indicating that the aerodynamic interference has small effects on the wind environment above the upper deck surface. Near the deck surface, the wind velocity becomes small within a certain height which is called the affected height. The affected height increases along the flow direction from lane 1 to lane 6.

However, the aerodynamic interference has significant effects on the wind environment above the lower deck surface. The wind profiles for the six lanes are different from those above the single box girder. For lanes 1-3 on the windward side, the wind velocities

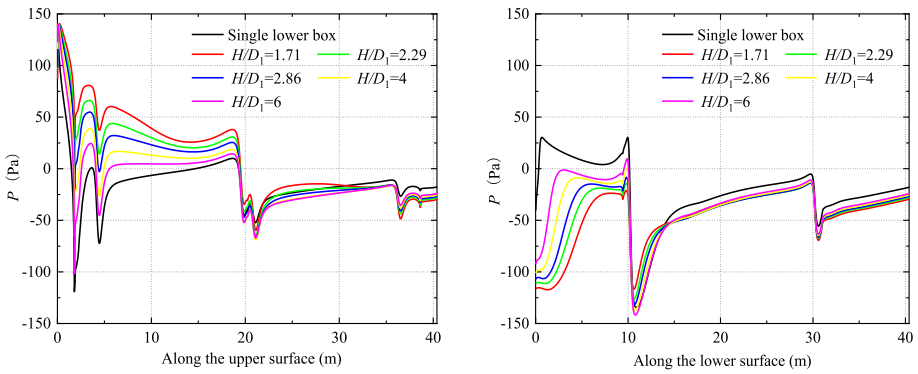

(a) on the upper surface (b) on the lower surface

Fig. 11 Distributions of the static pressure on the lower box

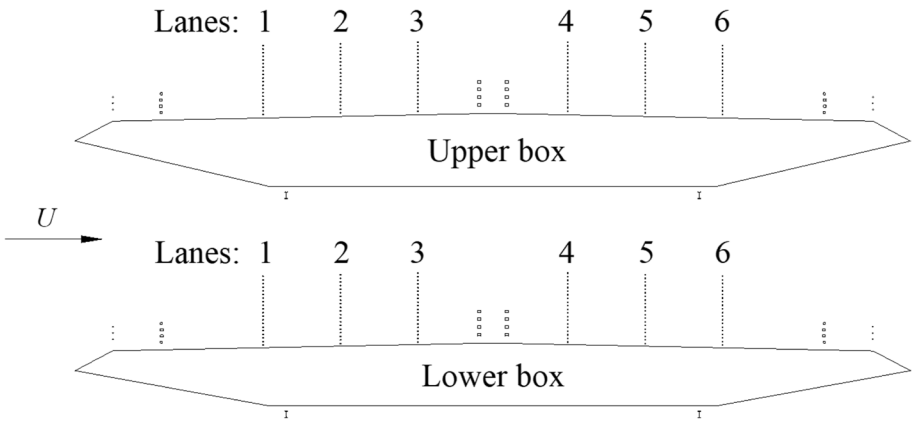

Fig. 12 Lanes above the deck surfaces

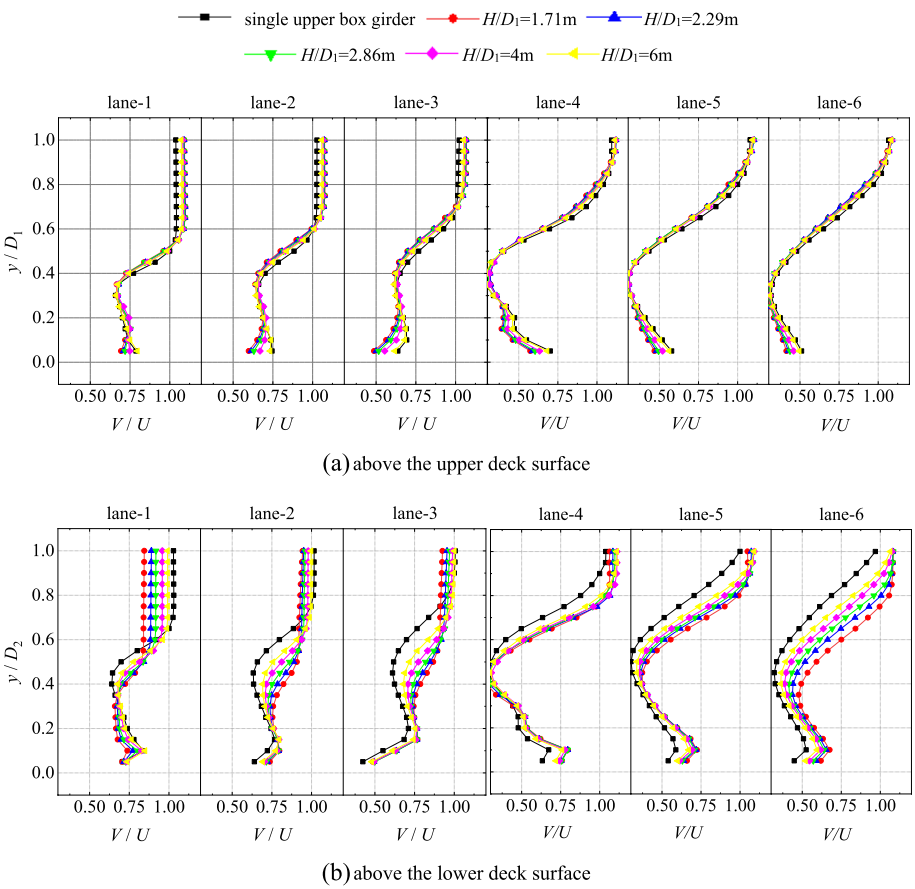

(a) above the upper deck surface

(b) above the lower deck surface

Fig. 13 Wind profiles of the normalized mean streamwise velocities

within the affected heights increase while the wind velocities above the affected heights decrease. For lanes 4-6 on the leeward side, as the affected heights become higher, the wind velocities within the computed heights increase.

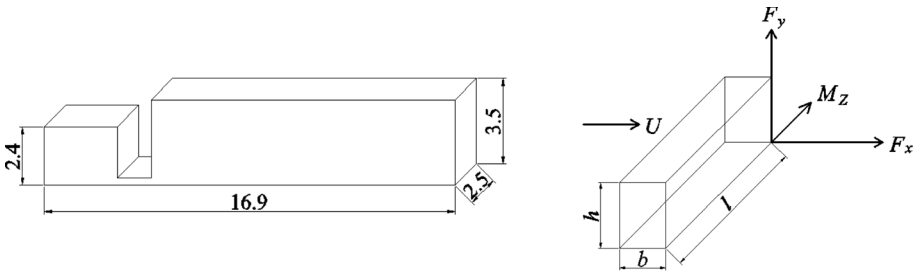

(a) Simplified vehicle mode (unit: m) (b) aerodynamic forces

Fig. 14 Descriptions on the simulated vehicle

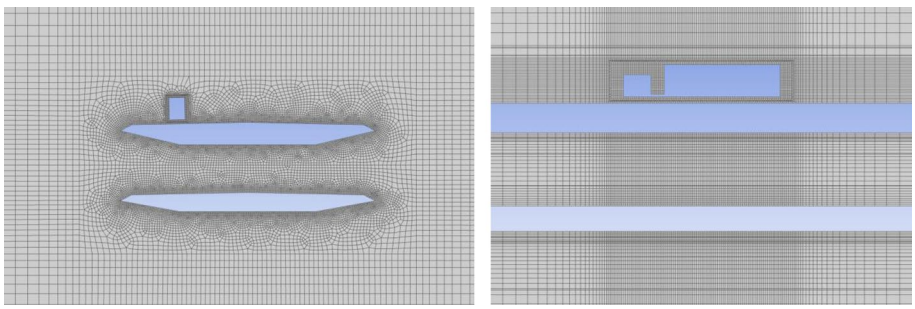

(a) in the *xy* plane (b) in the *yz* plane

Fig. 15 Local computational mesh around the vehicle

4.2 Aerodynamic forces on vehicles

The increasing wind velocities between the two boxes is unfavorable to the safety of vehicles travlling through the bridge. In this section, vehicles are considered in the CFD simulations in order to extract the aerodynamic forces. As discussed in introduction, the container car is easier to affect by strong winds which is taken as the target here. The simulated size of the container car is shown in Fig. 14(a). In the three-dimensional CFD simulations, the vehicle is static, and the secondary elements of the bridge are not considered, such as crash barriers and railings. The scale ratio of 1:50 is adopted in the simulations. When the vehicle is located in lane1 above the upper box girder, local computational mesh is shown in Fig. 15. The computational domain is discretized by hexahedral cells. Both in the *xy* plane and *yz* plane, that is, in the transverse and longitudinal directions, more cells were generated around the vehicle. The total cell number in the computation domain is 3,244,353, and the quality of cell is relatively good as the maximum equisize skew value is 0.679. The windward and leeward faces are set as velocity-inlet and pressure-outlet boundaries, respectively. The vehicle and the girders are set as smooth walls.

The aerodynamic forces acting on the vehicle include lateral force F_x, lift force F_y, drag force F_z, deflection moment M_y, overturning moment M_z, and pitching moment M_x. For what concerns the running safety of vehicles, lateral force F_x, lift force F_y, and overturning moment M_z should be carefully studied. The lateral force, lift, and overturning moment coefficients are defined by the following equations.

$$C_d = F_x/\left(0.5\rho U^2 hl\right) \tag{4}$$

$$C_l = F_y/\left(0.5\rho U^2 bl\right) \tag{5}$$

$$C_m = M_z/\left(0.5\rho U^2 b^2 l\right) \tag{6}$$

where, C_d, C_l and C_m are the lateral force coefficient, lift coefficient and overturning moment coefficient respectively; h, b and l are the vehicle height, width, and length, respectively; U is the mean wind velocity and is set as 15 m/s here. The positive directions of forces are shown in Fig. 14(b).

The aerodynamic forces on the static vehicle were extracted by CFD simulations. When the vehicle is placed on lanes 1-3 above the upper and lower deck surfaces, respectively, the aerodynamic forces are shown in Fig. 16 where the abscissa is represented by the lateral position which is the distance from the vehicle to the windward sides of box girders.

From lane 1 to lane 3, the lateral force coefficient, lift coefficient and overturning moment coefficient of the vehicle decrease. Comparing the upper and lower lanes, the aerodynamic coefficients of the vehicle are larger when it is placed above the lower deck surface. The variations in aerodynamic coefficients are relatively significant as well.

When the vehicle is placed on lanes 1-3, respectively, the counters of the mean velocity are compared. Taking different cross sections of the vehicle as examples, the counters are shown in Figs. 17, 18 and 19. Blocked by the vehicle, the wind velocity in the wake decreases significantly, especially for 1/4, 1/2, and 3/4 positions. When the vehicle is placed above the upper deck surface, the flow could pass through the vehicle from its upper side as the space is large enough, so the acceleration effect is not significant. When the vehicle is placed above the lower deck surface, however, the space of the upper side is limited due to the existence of the upper box, so the flow acceleration becomes significant. Therefore, the aerodynamic forces on the vehicle are larger when it is placed above the lower deck surface. From lane 1 to lane 3, the acceleration effect above the vehicle gradually weakens.

The counters of the static pressure on the vehicle are further shown in Fig. 20. Comparing the two cases when the vehicle is placed on the upper and lower deck surfaces,

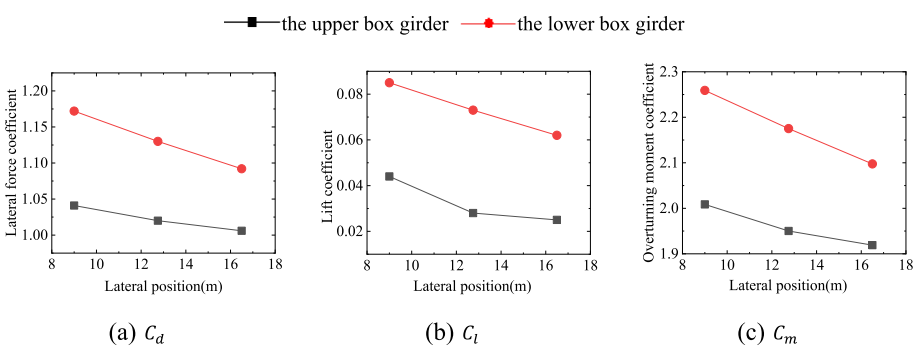

(a) C_d (b) C_l (c) C_m

Fig. 16 Aerodynamic coefficients of the vehicle

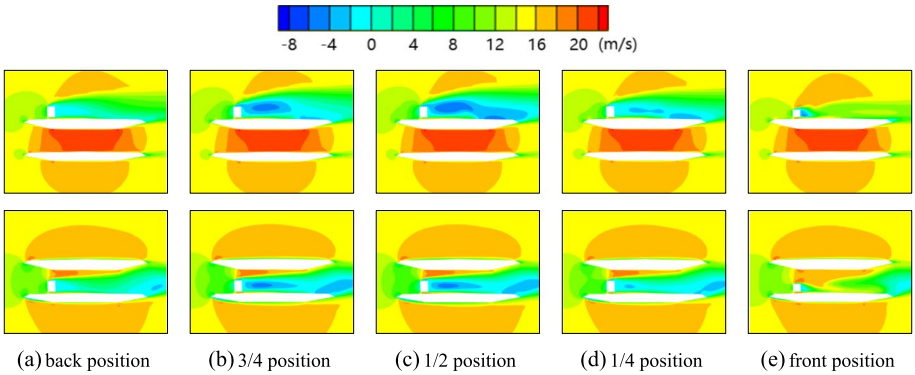

Fig. 17 Counters of the mean velocity for different cross sections (vehicle on lane 1)

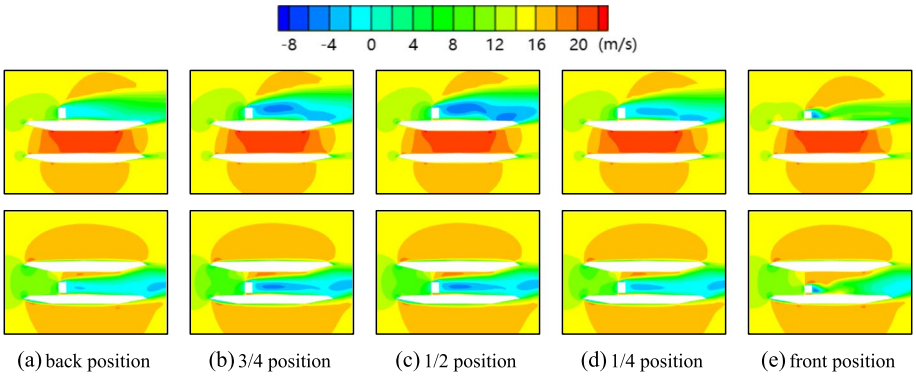

Fig. 18 Counters of the mean velocity for different cross sections (vehicle on lane 2)

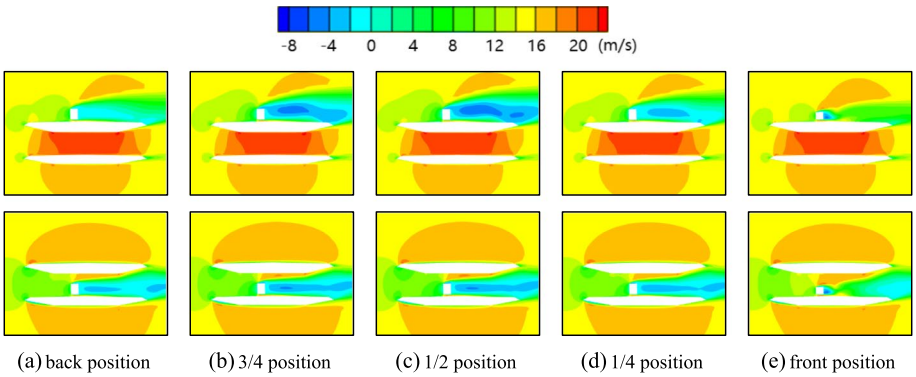

Fig. 19 Counters of the mean velocity for different cross sections (vehicle on lane 3)

the positive pressure on the windward surface of the vehicle is similar, while the negative pressure on the upper and leeward surfaces is different due to the wake flow.

5 Conclusions

The aerodynamic characteristics of a double-deck box girder are investigated. The effect of the aerodynamic interference between the two boxes on the aerodynamic coefficients is discussed. The flow field characteristics around the girder and the aerodynamic forces on a container car are further studied. The following conclusions are made.

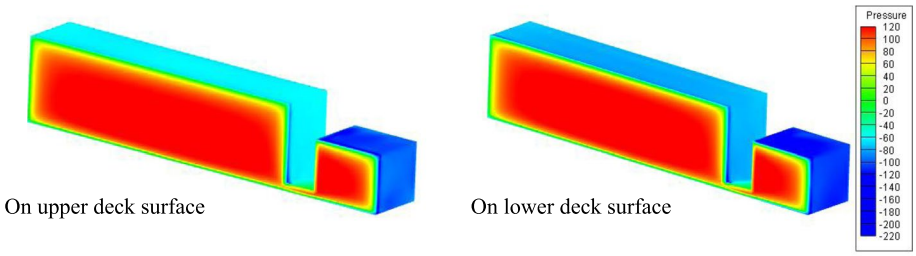

(a) pressure distribution on the windward surface (unit: Pa)

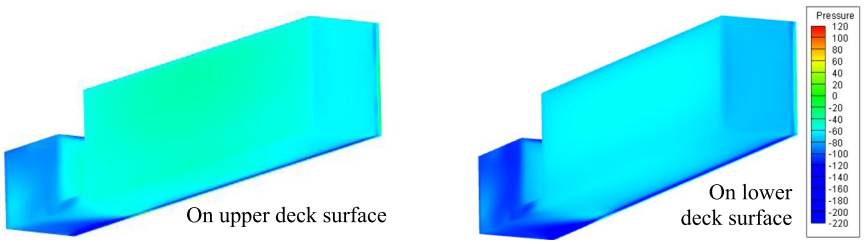

(b) pressure distribution on the leeward surface (unit: Pa)

Fig. 20 Counters of the mean velocity for different cross sections (vehicle on lane 3)

(1) For the two boxes in parallel arrangement, the aerodynamic coefficients change significantly due to the aerodynamic interference between them. As a large positive pressure region is formed between the two boxes, the lift and moment coefficients of the upper box are always larger than those of the lower box. For the entire girder, the variations in aerodynamic coefficients are similar with those of the single upper or lower box.

(2) The aerodynamic interference phenomenon is closely related to the angle of attack of approaching and the distance between the two boxes. With the increasing positive or decreasing negative angle of attack, the vortex above the upper box or below the lower box has a larger size due to the flow separation and the aerodynamic interference is more complex. With the increasing distance, the aerodynamic interference gradually weakens but it cannot be ignored even when H/D_1 increases to 6.

(3) The aerodynamic interference has small and significant effects on the wind environment above the upper and lower deck surfaces, respectively. Comparing the upper and lower lanes, the aerodynamic coefficients of the vehicle are larger when it is placed above the lower deck surface. The difference in aerodynamic forces is more related to the negative pressure on the upper and leeward surfaces of the vehicle.

Acknowledgments
The authors are grateful for the financial support from Natural Science Foundation of Sichuan Province (No. 2022NSFSC0004).

Authors' contributions
Shuwen Fan: Conceptualization, Methodology, Software, Formal analysis, Investigation, Writing - Original Draft. Wei Chen: Software, Validation, Formal analysis, Investigation, Writing - Original Draft, Visualization. Haojun Tang: Conceptualization, Writing - Review & Editing, Visualization, Supervision. Yongle Li: Resources, Project administration, Funding acquisition. The author(s) read and approved the final manuscript.

Funding
This study is supported by the Natural Science Foundation of Sichuan Province (No. 2022NSFSC0004).

Availability of data and materials
The data in current study are available from the corresponding author on reasonable request.

Declarations

Competing interests
Yongle Li is an editor-in-chief for Advances in Bridge Engineering and was not involved in the editorial review, or the decision to publish, this article. All authors declare that there are no competing interests.

Received: 2 November 2022 Accepted: 20 November 2022
Published online: 05 December 2022

References

Chen Z, Lin Z, Tang H, Li Y, Wang B (2019) Wake effects of an upstream bridge on aerodynamic characteristics of a downstream bridge. Wind Struct 29(6):417–430
de Miranda S, Patruno L, Ricci M, Ubertini F (2015) Numerical study of a twin box bridge deck with increasing gap ratio by using RANS and LES approaches. Eng Struct 99(15):546–558
Fang C (2014) The long-span bridge aerodynamic stability evaluation and application based on the static aerodynamic coefficient. Chang'an University, Xi'an (in Chinese)
Haque MN, Katsuchi H, Yamada H, Nishio M (2016) Investigation of edge fairing shaping effects on aerodynamic response of long-span bridge deck by unsteady RANS. Arch Civ Mech Eng 16(4):888–900
He X, Kang X, Yan L, Flay RGJ, Ren P, Wu T (2021) Numerical investigation of flow structures and aerodynamic interference around stationary parallel box girders. J Wind Eng Ind Aerodyn 215:104610
Huang L, Liao H, Wang B, Li Y (2009) Numerical simulation for aerodynamic derivatives of bridge deck. Simul Model Pract Th 17:719–729.
Li YL, Chen XY, Yu CJ, Togbenou K, Wang B, Zhu LD (2018) Effects of wind fairing angle on aerodynamic characteristics and dynamic responses of a streamlined trapezoidal box girder. J Wind Eng Ind Aerodyn 177:69–78
Liu Z, Zhang X, Chen T, Liu Y, Lu B (2022) Aerodynamic loads and bridge responses under train passage: case study of an overpass steel box-girder cable-stayed bridge. Adv Bridge Eng 3:1
Ogawa K, Shimodoi H, Oryu T (2002) Aerodynamic characteristics of a 2-box girder section adaptable for a super-long span suspension bridge. J Wind Eng Ind Aerodyn 90(12-15):2033–2043
Ricciardelli F (2003) On the wind loading mechanism of long-span bridge deck box sections. J Wind Eng Ind Aerodyn 91:1411–1430
Sato H, Kusuhara S, Ogi K, Matsufuji H (2000) Aerodynamic characteristics of super long-span bridges with slotted box girder. J Wind Eng Ind Aerodyn 88:297–306
Wang D, Zhang Y, Sun M, Chen A (2020) Characteristics of the wind environment above bridge deck near the pylon zone and wind barrier arrangement criteria. Appl Sci 10:1437
Wu B, Xue G, Feng J, Laima S (2021) The effects of aerodynamic interference on the aerodynamic characteristics of a twin-box girder. Appl Sci 25(8):04020053
Zhang J, Zhang M, Li Y, Qian Y, Huang B (2020) Local wind characteristics on bridge deck of twin-box girder considering wind barriers by large-scale wind tunnel tests. Nat Hazards 103:751–766
Zhou Q, Zhu LD (2020) Numerical and experimental study on wind environment at near tower region of a bridge deck. Heliyon. 6(5):e03902
Zhou R, Yang YX, Zhang L, Ge YJ (2017) Interference effect on stationary aerodynamic performance between parallel bridges. Int J Struct Stab Dyn 17(2):1750017

Publisher's Note